Transactions of the **14th International Conference on Structural Mechanics in Reactor Technology** (SMiRT 14), Lyon, France, August 17-22, 1997

3D experimental and numerical investigations to test constitutive equations for nonproportional cyclic plasticity

Calloch S., Marquis D.
ENS Cachan / LMT, France

ABSTRACT: This paper is concerned with the mechanical behavior of type 316 austenitic Stainless Steel under triaxial tension-compression cyclic loading. A triaxial tension-compression test devoted to the study of cyclic plasticity under non-proportional loadings is presented. Because the stress state in the central part of our triaxial specimen is not perfectly homogeneous, the interpretation of the tests needs 3D finite element analysis. The triaxial cyclic test developed is simulated with two sets of constitutive equations deduced from a large base of complex tension-torsion tests. The comparison between the structural analysis and the experimental results is made in order to determine the prediction capacity of the two models used.

INTRODUCTION

It is well-known that cyclic strain hardening along multiaxial non-proportional paths is much more significant than that along proportional one [1]. A great number of phenomenological models have been developed these ten last years in order to describe overhardening due to the non-proportionality of the loading path. The main idea consists in modifying the isotropic hardening rule [2], or the kinematic hardening rule or both isotropic and kinematic hardening rules [3] with an introduction of a non-proportional parameter defined as a relation between stress, inelastic strain, kinematic variable, and their rates, [2], or through a definition of a structural tensor [4].
The main goal of our work is to get more general experimental results in triaxial tension-compression cyclic test in order to test the accuracy of the constitutive equations identified on a large base of complex tension-torsion tests. In the first part of this paper, a presentation of two sets of constitutive equations for general cyclic plasticity is made. Then, a triaxial cyclic tension-compression test and the experimental results are presented. Finally, the triaxial cyclic test developed is simulated with a 3D finite element calculation with the two sets of constitutive equations mentioned above. The comparison between the structural analysis and the experimental results is made to determine the prediction capacity of the two models used.

CONSTITUTIVE EQUATIONS FOR GENERAL CYCLIC PLASTICITY

Description of the two models used

In this part, a particular attention is paid to model the additional hardening due to the loading path shape observed by many investigators. The main experimental result is a classification of different loading paths by additional hardening which is a good basis to test a set of constitutive equations describing cyclic plasticity [5], [6], [7]. In the following two sets of constitutive equations have been considered. The first one is the LMTNP model [8] and the second one is the Tanaka's model [4]. They are briefly recalled.

Strain partition : $\varepsilon_{ij} = \varepsilon_{ij}^{e} + \varepsilon_{ij}^{p}$ with ε_{ij}^{e} : elastic strain, ε_{ij}^{p} : plastic strain (1)

Elastic law : $\sigma_{ij} = C_{ijkl}\,\varepsilon_{kl}^{e}$ with σ_{ij} : stress tensor, C_{ijkl} : elasticity operator (2)

Elastic domain : $f(\underline{\underline{\sigma}}, \underline{\underline{X}}, R) = J_2(\underline{\underline{\sigma}} - \underline{\underline{X}}) - R - k \le 0$ with k : initial yield stress (3)

$\underline{\underline{X}}$: kinematic hardening tensor, R : isotropic hardening

and
$$J_2(\underline{\underline{\sigma}} - \underline{\underline{X}}) = \left[\frac{3}{2}(S_{ij} - X_{ij})(S_{ij} - X_{ij})\right]^{\frac{1}{2}} \quad (4)$$

where
$$S_{ij} = \sigma_{ij} - \frac{1}{3}\sigma_{kk}\delta_{ij} \quad (5)$$

Plastic flow rule :
$$\dot{\varepsilon}_{ij}^{p} = \frac{3}{2}\dot{\lambda}\frac{S_{ij} - X_{ij}}{J_2(\underline{\underline{\sigma}} - \underline{\underline{X}})} \text{ with } \dot{\lambda} : \text{plastic multiplier} \quad (6)$$

Kinematic hardening rule : $\dot{X}_{ij} = c\left[a\,\dot{\varepsilon}_{ij}^{p} - \varphi(p)\,X_{ij}\,\dot{p}\right]$ with c, a : material parameters (7)

and p : accumulated plastic strain

and $\varphi(p) = \varphi_{\infty} + (\varphi_0 - \varphi_{\infty})\,\exp(-\omega p)$ with φ_0, φ_{∞}, ω : material parameter (8)

Isotropic hardening rule : $\dot{R} = \gamma(Q - R)\dot{p}$ with γ : material parameter (9)

	LMTNP	TANAKA
Evolution of Q (saturated value of the isotropic hardening variable)	$\dot{Q} = D(A)\,[Q_{as}(A) - Q]\,\dot{p}$ where $D(A) = (d - f)\,A + f$ and $Q_{as}(A) = \dfrac{gAQ_{\infty} + (1-A)Q_0}{gA + (1-A)} + \left[A^n(1-A) + A(1-A)^n\right]Q_i$	$Q = A[q_N(q) - q_P(q)] + q_P(q)$ with $\begin{cases} \dot{\vec{Y}} = r_Y(\vec{E}^p - \vec{Y})\,\dot{p} \\ q = \lVert \vec{E}^p - \vec{Y} \rVert \end{cases}$ and $q_P(q) = a_P\,q + b_P\{(1 - \exp(-c_P\,q))\}$ $q_N(q) = a_N\,q + b_N\{(1 - \exp(-c_N\,q))\}$
Definition of the non-proportional parameter, A	$A = 1 - \cos^2\alpha$ with : $\cos\alpha = \dfrac{X_{ij}\,\dot{X}_{ij}}{[X_{ij}\,X_{ij}]^{\frac{1}{2}}\,[\dot{X}_{ij}\,\dot{X}_{ij}]^{\frac{1}{2}}}$	$A = \sqrt{\dfrac{Tr(\underline{\underline{C}}^T\underline{\underline{C}}) - \vec{u}\,\underline{\underline{C}}^T\underline{\underline{C}}\,\vec{u}}{Tr(\underline{\underline{C}}^T\underline{\underline{C}})}}$ Structural tensor : $\dot{\underline{\underline{C}}} = c_c\left[\left(\dfrac{\dot{\vec{E}}^p}{\lVert\dot{\vec{E}}^p\rVert} \otimes \dfrac{\dot{\vec{E}}^p}{\lVert\dot{\vec{E}}^p\rVert}\right) - \underline{\underline{C}}\right]\dot{p}$ with $\vec{E}^p : \begin{cases} E_1 = \varepsilon_{11}^p \\ E_2 = \dfrac{2}{\sqrt{3}}\left[\varepsilon_{11}^p/2 + \varepsilon_{22}^p\right] \\ E_3 = 2\,\varepsilon_{12}^p/\sqrt{3} \\ E_4 = 2\,\varepsilon_{23}^p/\sqrt{3} \\ E_5 = 2\,\varepsilon_{31}^p/\sqrt{3} \end{cases}$

Identification of material parameters

The two present models, LMTNP and Tanaka's model, include 15 and 16 material parameters respectively. In the following we discuss the determination of these materials constants. For this purpose an numerical approach has been used.

The material parameters, E, ν, k, Q_0, φ_∞, ω, C and $(\varphi_0-\varphi_\infty)$ for LMTNP model and E, ν, k, a_p, b_p, c_p, φ_∞, ω, C and $(\varphi_0-\varphi_\infty)$ for Tanaka's model, have been evaluated with a cyclic uniaxial loading. The comparison between experimental and numerical results is given in figure 1. The material parameters Q_∞, d, Q_i, n, d, g and f for LMTNP model and C_c, a_N, b_N, c_N and r_Y for Tanaka's model have been identified with a cyclic 90° out-of-phase loading, a cyclic butterfly loading and a cyclic clover loading. The shapes of these three loading paths are given in figure 4. The comparison between experimental and numerical results is given in figure 2 and 3 and the material data for 316 SS used are given in table 1 and 2. After the identification of material constants, a large base of tension-torsion cyclic loading has been simulated. The comparisons between the maximum Von Mises equivalent stress at steady state given by the two models and the experimental results are given in figure 4.

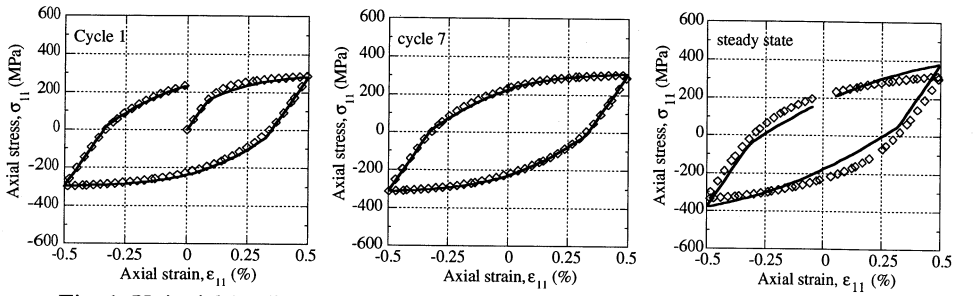

Fig. 1: Uniaxial loading - comparison between experimental and numerical results.
—— *simulation (for the two models), ◊ experimental results*

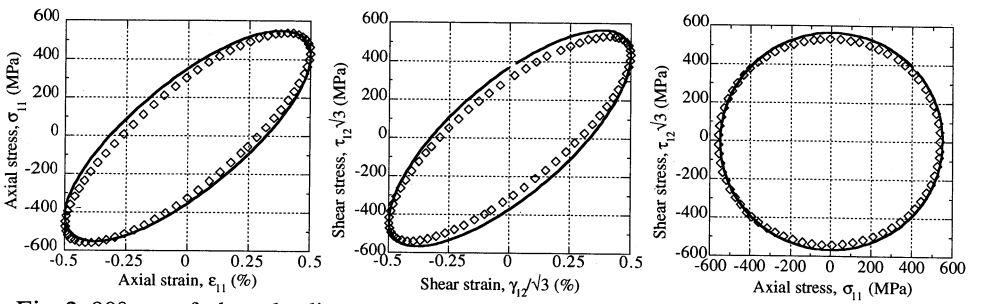

Fig. 2: 90° out-of-phase loading - comparison between experimental and numerical results.
—— *simulation (for the two models), ◊ experimental results*

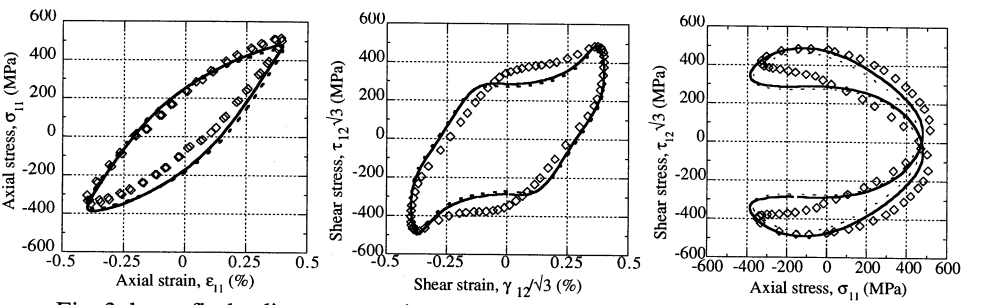

Fig. 3: butterfly loading - comparison between experimental and numerical results.
—— *simulation (LMTNP model),, - - - simulation (Tanaka's model), ◊ experimental results*

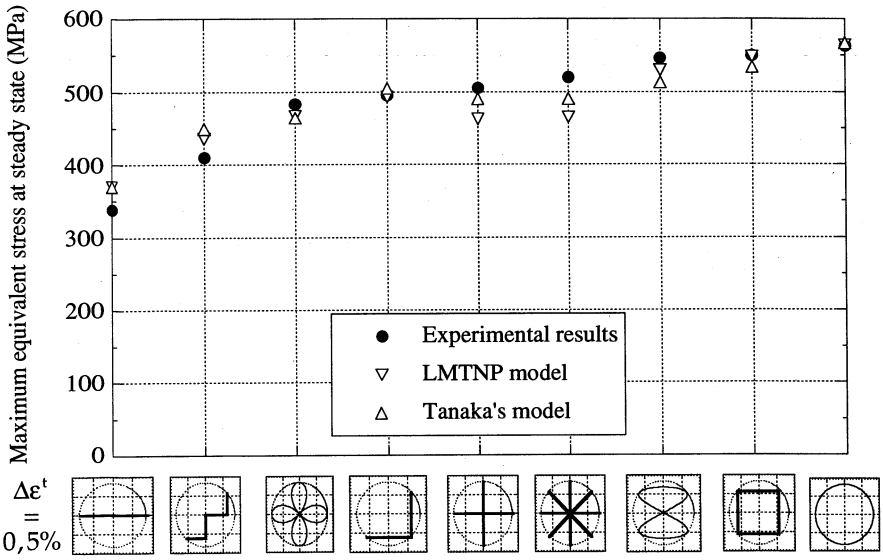

Fig. 4: Comparison between experimental results and simulations for different loadings

E = 187 000 MPa	Q_0 = 0 MPa	d = 90	ω = 10,0
ν = 0,33	Q_∞ = 214 MPa	g = 0,1	C = 61845 MPa
k = 160 MPa	Q_i = 2334 MPa	φ_∞ = 0,48 E-02	$(\varphi_0-\varphi_\infty)$ = 0,65 E-02
γ = 32	n = 8,26	f = 0,85	

Table 1: LMTNP model, material data for 316 Stainless Steel at room temperature.

E = 187 000 MPa	γ = 32	a_P = 0	φ_∞ = 0,48 E-02
ν = 0,33	a_N = 77300	b_P = 0	$(\varphi_0-\varphi_\infty)$ = 0,65 E-02
k = 160 MPa	b_N = 50,7	c_P	ω = 10
c_C = 2,1	c_N = 6377,7	C = 61845 MPa	r_Y = 40,75

Table 2 : Tanaka's model, material data for 316 Stainless Steel at room temperature.

DESCRIPTION OF THE TRIAXIAL TEST

Experimental equipment

The basic idea of this test is to load a cube of material in tension-compression along three perpendicular directions [9]. To achieve this loading a testing machine with six servohydraulic actuators (see Fig. 5) is used. These actuators are coupled two by two on three perpendicular axis. The specimen is fixed to the actuators through six identical grips (see Fig. 6). The fixation of the specimen on the grips and the fixation of the grips on the actuators are made by screws. The control system is such that the central point of the specimen is motionless avoiding the coupling between the different axis of the specimen.

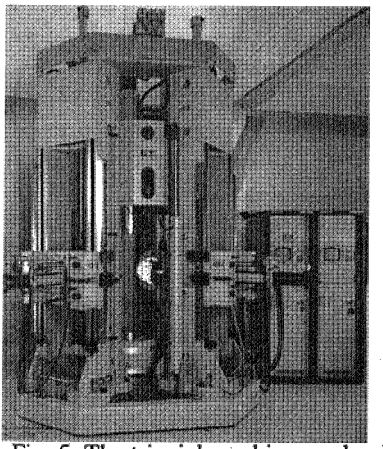

Fig. 5: The triaxial machine used.

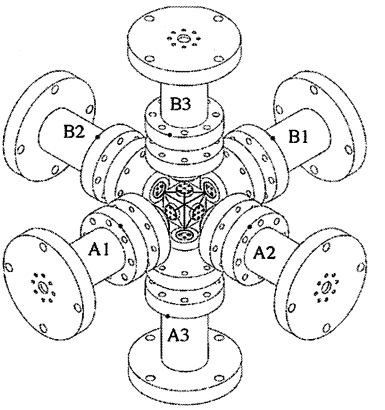

Fig. 6: The specimen and the six grips

Triaxial specimen

The specimen, (see Fig. 7 and 8), is made of a cube linked to the grips by six pyramidal frustums [9]. The specimen, made of 316 SS, were machined from bars. The heat treatment of the bars is a one hour soaking at 1050°C followed by a quench in water to ensure the initial isotropy of the material.

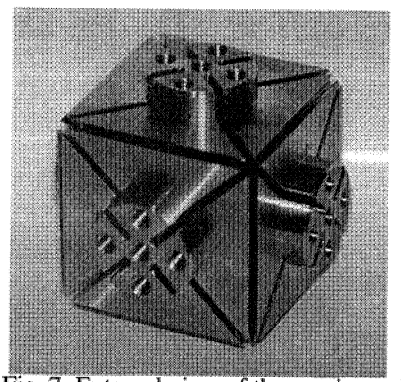

Fig. 7: External view of the specimen.

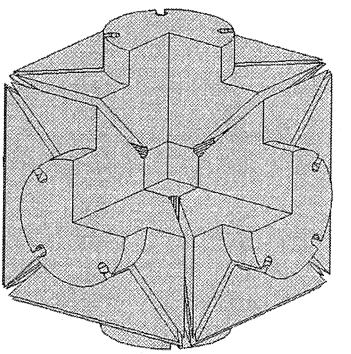

Fig. 8: Internal view of the specimen

Description of loading path

The loading is applied to the specimen with two control loops, the main one is under load control, the second one is under amplitude displacement control. In other words and for each axis, the load-displacement loop is load controlled. The load is applied until a limited value in displacement is reached. After reaching this limit, the load direction is inverted. The same absolute value of displacement limit for loading and off-loading is chosen.

In this specific test the specimen is loaded in one direction, (axis), off-loaded and reloaded till zero load. Afterwards, the same strategy is applied on the second axis then on the third axis. Thus, one cycle is constructed with three branches in the load space (F_1, F_2, F_3) (see Fig. 9). Then, because of the cyclic hardening phenomenon in the material, the peak load increased in magnitude up to the cyclic stabilization (see Fig. 9). A maximum load of 15 kN was reached at the first cycle and a maximum load of 20 kN was reached at steady state. Then an increase of peak load of 33 % has been observed.

STRUCTURAL ANALYSIS OF THE TEST

In so far as the geometry of our specimen is complex, the deduction of the stress from the loads and of the strains from the displacements is not direct. Then, a three dimensional structural analysis based on finite element method is necessary to analyse the test.
A mesh is used for the spacial modelling of the specimen. Advantage is taken of the symmetry characteristics of the problem. The mesh consisted of 17 619 degrees of freedom and 14 757 elements, modelled an eighth of the specimen (see Fig. 10). Then symmetry boundary conditions were used and the loading was applied on the external circular faces of the mesh (FCLx, FCLy and FCLz) (see Fig. 11) as the one described in the experimental procedure part.

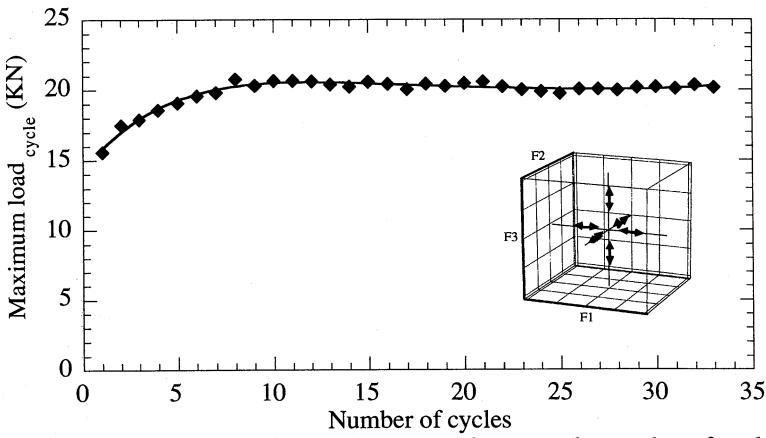

Fig. 9: Evolution of the maximum load per cycle versus the number of cycle.

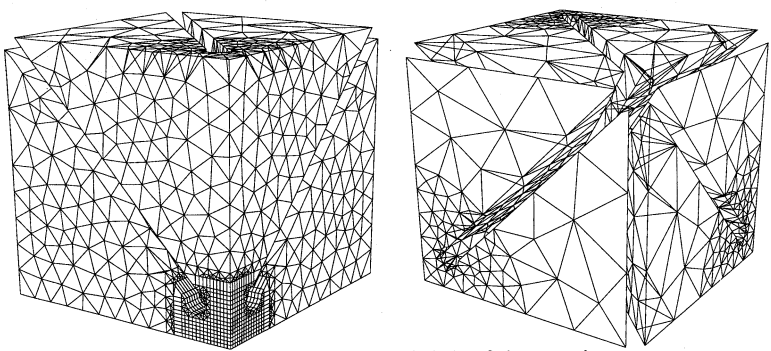
Fig. 10: The mesh of an eighth of the specimen.

Seven cycles have been simulated using the two sets of constitutive equations presented above. The comparison of the evolution of the maximum load versus the number of cycles between the experimental and numerical results is given in figure 12. The numerical simulations exhibit a good agreement with the first experimental cycle. But they underestimate the evolution of the maximum load when the number of cycles increases (see Fig. 12). Clearly the model developed by Tanaka leads to better results with such a loading. The difference between the two simulation results is due to the difference in the definition of the non-proportional parameter. At figure 13, the evolution at the center of the specimen of the isotropic hardening variable is reported for the two models. It is clear that the model LMTNP for such a loading leads to very low values of the parameter A and of the isotropic

hardening variable. Conversely, the Tanaka's model with its definition of parameter A based on a structural tensor leads to higher values of A for this loading and consequently to higher values of the isotropic hardening.

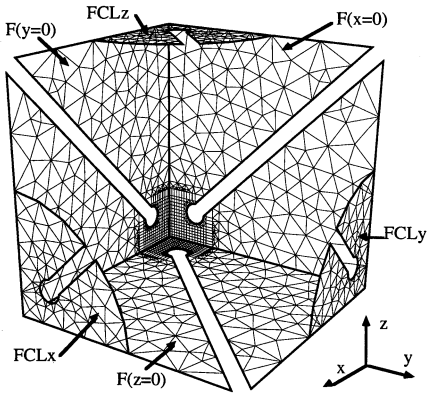

Fig. 11 : Description of boundary conditions.

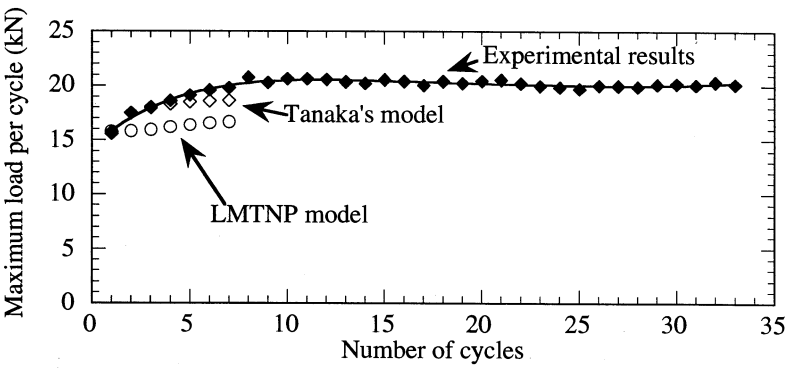

Fig. 12 : Evolution of the maximum load *versus* the number of cycles, experimental an numerical results.

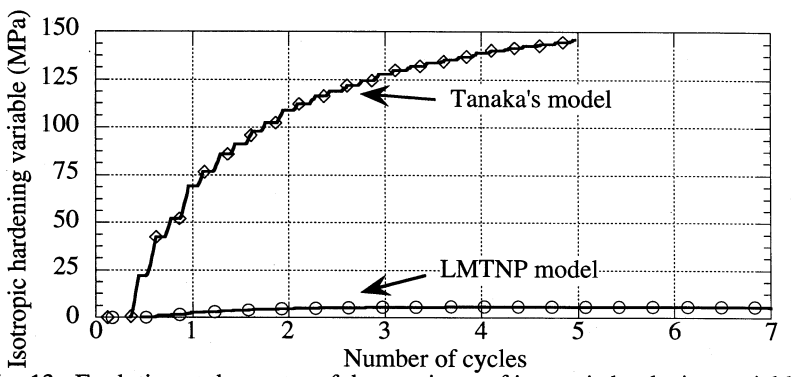

Fig. 13 : Evolution at the center of the specimen of isotropic hardening variable.

CONCLUSION

Two models for non-proportional plasticity has been described in a first part. This models give satisfying results for modelling the additional hardening phenomenon due to the loading path shape in tension-torsion. Then, a triaxial tension-compression cyclic test has been presented and developed in order to check or validate the previous constitutive equations. After a 3D finite element calculation, the main conclusion is that although the models used are good for very different non-proportional tension-torsion cyclic loadings, under triaxial loading they underestimate the evolution of the maximum load when the number of cycles increases. Then, certain definite conclusions can be drawn from this experimental and numerical investigations. First, a revision of the model used is necessary for a good description of the triaxial experimental observations. Secondly, this analysis can be generalised for the other models developed for cyclic plasticity and then conclusions about their performances in this case of loading path will be drawn.

REFERENCES

1. Lamba, H.S., Sidebottom, O. M., 1978. Cyclic Plasticity for Nonproportional Paths, Part I: Experiment, ASME, *Journal of Engineering Materials and Technology*, Vol. 100, pp. 96-103.
2. Benallal, A., Marquis, D., 1987. Constitutive Equations for Nonproportional Cyclic Elasto-Viscoplasticity, ASME, *Journal of Engineering Materials and Technology*, Vol. 109, pp. 326-336.
3. Abdul-Latif, A., Clavel, M., Ferney, V., Saanouni, K., 1994. On the Modelling of Nonproportional Cyclic Plasticity of Waspaloy, ASME, *Journal of Engineering Materials and Technology*, Vol. 116, pp. 35-43.
4. Tanaka E., 1994. A Nonproportionality Parameter and a Viscoplastic Constitutive Model Taking into Account Amplitude Dependence and Memory Effects of Isotropic Hardening. *European Journal of Mechanics, and Solids,* 13, 155-173.
5. Benallal, A., Le Gallo, P., Marquis, D., 1989. An Experimental Investigation of Cyclic Hardening of 316 Stainless Steel and of 2024 Aluminium Alloy Under Multiaxial Loadings, *Nuclear Engineering and Design*, Vol. 114, pp. 345-353.
6. Calloch, S., Marquis, D., 1997. Additional Hardening due to Tension-Torsion Nonproportional Loadings : Influence of the Loading Path Shape, Multiaxial Fatigue and Deformation Testing Techniques, ASTM STP 1280, S. Kalluri and P. J. Bonacuse, Eds, pp. 113-130.
7. Tanaka, E., Murakami, S., Ooka, M., 1985. Effects of Strain Paths Shapes on Nonproportional Cyclic Plasticity, *J. Mech. Phys. Solids*, Vol. 33, pp. 559-575.
8. Calloch, S., Marquis, D., 1996, Triaxial Tension-Compression Loadings in Cyclic Elasto-Plasticity : Experimental and Numerical Aspects, Proceedings of the 3rd Asia-Pacific Symposium on Advances in Engineering Plasticity and its Applications, Ed. Abe, T., Tsuta, T., Japon, pp. 135-141.
9. Calloch, S., 1997. Essais Triaxiaux Non-proportionnels et Ingénierie des Modèles de Plasticité Cyclique, Thèse de doctorat de l'École Normale Supérieure de Cachan.